

Green's functions of multiband non-Hermitian systems

Yu-Min Hu^{1,2} and Zhong Wang¹

¹*Institute for Advanced Study, Tsinghua University, Beijing, 100084, China*

²*Department of Physics, Princeton University, Princeton, NJ 08544, USA*

(Dated: May 1, 2023)

Green's functions of non-Hermitian systems play a fundamental role in various dynamical processes. Because non-Hermitian systems are sensitive to boundary conditions due to the non-Hermitian skin effect, open-boundary Green's functions are closely related to the non-Bloch band theory. While the exact formula of open-boundary Green's functions in single-band non-Hermitian systems proves to be an integral along the generalized Brillouin zone (GBZ), the proper generalization in generic multiband systems remains unclear. In this work, we derive a formula of open-boundary Green's functions in multiband non-Hermitian systems by viewing the multiband GBZ on the Riemann surface. This formula can be applied to describe directional amplification in multiband systems, which can be verified at various experimental platforms.

I. INTRODUCTION

Numerous intriguing properties emerging in non-Hermitian systems have attracted increasing attention [1, 2]. One of the fascinating non-Hermitian features is non-Hermitian skin effect (NHSE), where bulk states under open boundary conditions (OBC) accumulate at the boundaries [3–15]. NHSE invalidates conventional Bloch-band picture and leads to the non-Bloch band theory based on the generalized Brillouin zone (GBZ) [3, 16]. Initially developed to elucidate non-Hermitian topology [3–5, 16–25], the non-Bloch band theory also underlies various non-Hermitian dynamical phenomena [26–32].

To study the responses to external perturbations in a non-Hermitian system with NHSE, OBC Green's functions in one-dimensional single-band models and some simple multiband models have been formulated as a contour integral on the GBZ [33–35]. The GBZ-based formula can be easily evaluated by residue theorem, the results of which have been applied to directional amplification [33] and topological quantized response [36].

Despite the fundamental significance of non-Hermitian Green's functions, there is currently no proper generalization of GBZ-based formulas in generic multiband non-Hermitian systems. One of the difficulties is that energy bands are multi-valued functions [37–40]. Additionally, multiband GBZ has complex substructures denoted by sub-GBZs [38]. As a result, multiband systems with complicated sub-GBZs exhibit many unique properties that are dramatically different from single-band models whose GBZ is a single loop. These differences complicate the direct generalization of GBZ-based Green's functions.

To address this problem, we develop the theory of non-Hermitian Green's functions in generic multiband systems from the perspective of the Riemann surface attached to the multi-valued energy function. Let us consider a generic multiband non-Hermitian Bloch Hamiltonian $h(k) = \sum_{n=-m}^m a_n e^{ikn}$, where a_{-m}, \dots, a_m are $l \times l$ hopping matrices between different unit cells with l being the number of orbitals in a unit cell. The real-space Hamiltonian H can be easily generated by $h(k)$. Our central result is the GBZ-based formula of the OBC Green's function $G(\omega) = \frac{1}{\omega - H}$ of multiband non-Hermitian

systems:

$$\langle x, a | G(\omega) | y, b \rangle = \sum_{j=1}^l \int_{\text{GBZ}_j} \frac{d\beta}{2\pi i \beta} \beta^{x-y} \frac{\langle a | R_j, \beta \rangle \langle L_j, \beta | b \rangle}{\omega - E_j(\beta)}, \quad (1)$$

where x, y are the spatial locations of different unit cells and a, b represent the internal orbitals in each unit cell. In the above equation, with the definition $h(\beta) \equiv h(e^{ik} \rightarrow \beta)$, we have $h(\beta) |R_j, \beta\rangle = E_j(\beta) |R_j, \beta\rangle$ and $\langle L_j, \beta | h(\beta) = \langle L_j, \beta | E_j(\beta)$ for general complex β . $|R_j, \beta\rangle$ and $|L_j, \beta\rangle$ with $j = 1, 2, \dots, l$ are biorthogonal eigenstates of $h(\beta)$. $E_j(\beta)$ is the eigenvalue of $h(\beta)$ on the j -th Riemann sheet of the Riemann surface. The Riemann surface in consideration consists of all the solutions (β, E) of the algebraic equation $\det(E - h(\beta)) = 0$, which form a one-dimensional complex subspace of the two-dimensional complex (β, E) space.

We shall derive this formula as an integral along sub-GBZs [GBZ_j in Eq. (1)] which is viewed on the Riemann surface rather than simply on the complex β -plane. To do this, we first investigate the properties of GBZ in multiband non-Hermitian systems. Concretely, on the Riemann surface determined by the characteristic equation $\det(E - h(\beta)) = 0$, multiband GBZ divides into several sub-GBZs that are attached to different Riemann sheets. These sub-GBZs are denoted by GBZ_j with j being the sheet index. Each sub-GBZ is associated with one non-Bloch band of the OBC spectrum. Crucially, the sub-GBZs form a boundary on the Riemann surface, separating the β roots of the characteristic equation into two distinct groups.

Based on these properties, we then formulate the multiband Green's functions by using contour deformation on each Riemann sheet. In the end, we obtain the GBZ-based formula Eq. (1), which provides asymptotically exponential behaviors that are analogous to those found in single-band systems or in simple multiband systems with overlapping sub-GBZs [33]. The formula is independent of artificial choices of frequency-dependent integral contours. It unveils the vital role of multiband sub-GBZs in non-Hermitian dynamics and elucidates the response properties of all energy bands in multiband systems. Given that Green's functions are closely related to experiments, our results are readily applicable to various experimental platforms where NHSE is observed [8–12].

This paper is organized as follows. In Sec. II, we first discuss the basic facts of the multiband GBZ from the perspec-

tive of the Riemann surface. Then in Sec. III, we derive the formula of multiband non-Hermitian Green's functions as an integral on the sub-GBZs. Finally, we conclude our work in Sec. IV.

II. GENERALIZED BRILLOUIN ZONE IN MULTIBAND NON-HERMITIAN SYSTEMS

To begin with, we consider a general non-Hermitian model with l energy bands. As introduced above, the $l \times l$ Bloch Hamiltonian is given by $h(k) = \sum_{n=-m}^m a_n e^{ikn}$ with a_{-m}, \dots, a_m being $2m+1$ hopping matrices with dimension l . A Hermitian multiband model is obtained if $a_{-n} = a_n^\dagger$. Due to the NHSE with OBC, it is convenient to define a non-Bloch Hamiltonian via replacing e^{ik} by a complex number β :

$$h(\beta) = \sum_{n=-m}^m a_n \beta^n. \quad (2)$$

Immediately, the characteristic equation of the OBC eigenequation $H|\psi\rangle = E|\psi\rangle$ is given by

$$\det(E - h(\beta)) = 0. \quad (3)$$

In general, this is an algebraic equation of both β and E . For each E , there are $2ml$ roots of β . They can be sorted by their norms: $|\beta_1(E)| \leq |\beta_2(E)| \leq \dots \leq |\beta_{2m}(E)|$. For later convenience, we define $M = ml$. In the non-Bloch band theory, the GBZ is determined by [3, 16]

$$|\beta_M(E)| = |\beta_{M+1}(E)|. \quad (4)$$

This equation originates from the requirement of OBC. The GBZ defined by Eq. (4) plays the same role in non-Hermitian systems as the conventional Brillouin zone in Hermitian systems.

While the results in this paper are quite general in multiband non-Hermitian systems, we employ a particular model as an illustrative example:

$$h(\beta) = \begin{pmatrix} (t_1 + \gamma_1)\beta + \frac{t_1 - \gamma_1}{\beta} + V & \delta \\ \delta & (t_2 + \gamma_2)\beta + \frac{t_2 - \gamma_2}{\beta} - V \end{pmatrix}. \quad (5)$$

The real-space Hamiltonian is presented in Fig. 1(a). This model describes two Hatano-Nelson models coupled by intracell hoppings. It was proposed to illustrate the critical NHSE when $\delta \rightarrow 0$ [37, 41, 42]. In our study, we focus on the general choices of parameters with nonzero δ and develop its OBC Green's functions below. This is a two-band model and its characteristic equation has four roots $|\beta_1(E)| \leq |\beta_2(E)| \leq |\beta_3(E)| \leq |\beta_4(E)|$. The GBZ equation is given by $|\beta_2(E)| = |\beta_3(E)|$. A typical GBZ of this model is shown in Fig. 1(c), which has substructures called sub-GBZs [38] (labeled by red/blue lines in the plot).

Interestingly, Eq. (3) is also a high-order algebraic equation of complex energy E . From this point of view, we can rewrite this equation as

$$\det(E - h(\beta)) = \prod_{j=1}^l (E - E_j(\beta)) = 0 \quad (6)$$

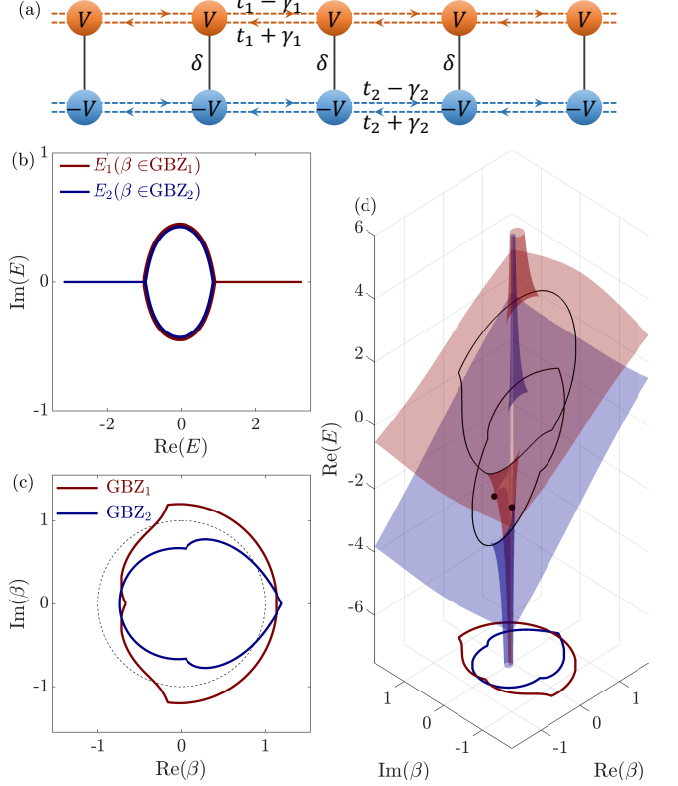


FIG. 1. (a) The model. (b) The OBC spectrum with two non-Bloch energy bands. (c) The GBZ with two sub-GBZs. Red/blue lines in (b) and (c) represent the sheet indexes of the Riemann surface. (d) The Riemann surface of these two bands with black lines being sub-GBZs on each Riemann sheet. The two black points are the branch points (exceptional points) connecting two sheets. Parameters: $t_1 = 1$, $\gamma_1 = -0.3$, $t_2 = 1$, $\gamma_2 = 0.5$, $\delta = 1$, $V = 0.8$. We keep these parameters throughout this paper.

where $E_1(\beta)$, $E_2(\beta)$, \dots , $E_l(\beta)$ are solutions of E at a given β . They are the l Riemann sheets of the whole Riemann surface. When β goes around the unit circle, $E_j(e^{ik})$ provides the Bloch spectrum of the j -th energy band with periodic boundary conditions.

The set $\{\beta, E_j(\beta)\}$ for arbitrary complex β forms the j -th sheet of the Riemann surface. In multiband non-Hermitian systems, there are in total l sub-GBZs for l energy bands, each of which lies on a Riemann sheet [38]. We label the sub-GBZ on the j -th sheet as GBZ_j . When β goes around GBZ_j , $E_j(\beta)$ produces the j -th non-Bloch energy band of the OBC spectrum. This is the non-Bloch generalization of the Bloch band structure.

In the characteristic equation, $2M$ roots $\beta_1(E), \dots, \beta_{2M}(E)$ correspond to a certain E . For each root $\tilde{\beta} \equiv \beta_k(E)$ with the root index $k \in \{1, \dots, 2M\}$, there are l different energies $E_1(\tilde{\beta}), \dots, E_l(\tilde{\beta})$ determined by Eq. (6). Among these, there should be a unique $E_j(\tilde{\beta}) = E$, except for some accidental degeneracy. It means that the solution set $\{\beta_k(E), E\}$ stays on the j -th Riemann sheet. By this procedure, a unique sheet index j is attached to each β root of Eq. (3). Then we can label these roots as $\beta_k^{(j)}(E)$, where k is the root index and j is the sheet

index determined by k . It is worthwhile to point out that for $2M$ roots of a certain E , the sheet index j does not necessarily cover all elements in $\{1, 2, \dots, l\}$ but the root index k always runs from 1 to $2M$. Moreover, the GBZ equation Eq. (4) can be written as

$$|\beta_M^{(j)}(E)| = |\beta_{M+1}^{(j')}(E)| \quad (7)$$

where j and j' generally take different sheet indexes. It means that $\{\beta_M^{(j)}(E), E\}$ and $\{\beta_{M+1}^{(j')}(E), E\}$ satisfying the above equation can belong to different Riemann sheets, contributing to GBZ_j and $\text{GBZ}_{j'}$ respectively, though they provide the same OBC energy.

As an illustration, we apply the multiband GBZ theory to the model in Fig. 1. The two-band model has two sub-GBZs, labeled by red and blue curves respectively in Fig. 1(c). The two Riemann sheets are shown in Fig. 1(d). Conveniently, we label the sheet with the red (blue) sub-GBZ as the first (second) sheet $E_1(\beta)$ ($E_2(\beta)$). Correspondingly, the red (blue) sub-GBZ is denoted by GBZ_1 (GBZ_2). When β goes around GBZ_1 (GBZ_2), the OBC spectrum $E_1(\beta)$ ($E_2(\beta)$) in Fig. 1(b) is shown by solid lines with the same colors. Notably, a part of the red and blue spectrums overlap on the loop of the OBC spectrum. When we take energy values from this loop, the corresponding GBZ equation is Eq. (7) with $j \neq j'$.

After putting multiband GBZ on the Riemann surface, we are ready to elucidate an important feature that multiband GBZ is a boundary separating the roots of the characteristic equation when E is not on the OBC spectrum.

To see this, we first review the results in single-band non-Hermitian systems [43, 44]. Given a typical single-band non-Bloch Hamiltonian $h(\beta) = \sum_{n=-M}^M t_n \beta^n$ with t_n being complex numbers, the characteristic equation $E - h(\beta) = 0$ has $2M$ roots $|\beta_1(E)| \leq \dots \leq |\beta_{2M}(E)|$ ordered by their norms. An elegant theorem states that the single-band GBZ is a boundary between $\{\beta_1(E), \beta_2(E), \dots, \beta_M(E)\}$ and $\{\beta_{M+1}(E), \beta_{M+2}(E), \dots, \beta_{2M}(E)\}$ for arbitrary E . This theorem comes from the fact that the OBC spectrum has a vanishing winding number. Namely, $W(E) \equiv \frac{1}{2\pi} \int_{\text{GBZ}} \frac{d}{d\beta} \log(E - h(\beta)) d\beta = 0$ when E is not on the OBC spectrum. Since the polynomial $E - h(\beta)$ has an order- M pole at the origin, there must be M zeros of $E - h(\beta) = 0$ inside the GBZ. A more careful analysis unveils that GBZ encircles $\{\beta_1(E), \beta_2(E), \dots, \beta_M(E)\}$ while the other M zeros with larger norms stay outside. In the end, the single-band GBZ is a boundary between $\{\beta_1(E), \beta_2(E), \dots, \beta_M(E)\}$ and $\{\beta_{M+1}(E), \beta_{M+2}(E), \dots, \beta_{2M}(E)\}$ for arbitrary E not on the OBC spectrum.

Now we discuss the analogous property for the GBZ in multiband non-Hermitian systems. While the fact that different sub-GBZs belong to different sheets makes it subtle to consider winding numbers of sub-GBZs, we can bypass this subtlety via the following argument. Starting from Eq. (3), we consider a large E far away from the OBC spectrum ($|E| \rightarrow +\infty$). In this limit, there are M roots $\{\beta_1^{(j_1)}(E), \dots, \beta_M^{(j_M)}(E)\}$ close to the origin and the other M roots $\{\beta_{M+1}^{(j_{M+1})}(E), \dots, \beta_{2M}^{(j_{2M})}(E)\}$ go to the infinity, no matter what sheets they belong to. Under this circumstance, all sub-

GBZs on different sheets naturally separate these $2M$ points $\{\beta_k^{(j_k)}(E), E\}$ on the Riemann surface.

Let us move E back from the infinity. At the same time, these $2M$ roots $\{\beta_k^{(j_k)}(E), E\}$ will move on the Riemann surface. During this process, the sheet indexes of these roots may change when E crosses some branch cuts on the Riemann surface. The order indexes may exchange within $\{\beta_1^{(j_1)}(E), \dots, \beta_M^{(j_M)}(E)\}$ or $\{\beta_{M+1}^{(j_{M+1})}(E), \dots, \beta_{2M}^{(j_{2M})}(E)\}$. As long as E does not pass the OBC spectrum, the point $\{\beta_k^{(j_k)}(E), E\}$ on the j_k -th sheet will not cross the GBZ_{j_k} . Even though a point $\{\beta_{k'}^{(j_{k'})}(E), E\}$ on the $j_{k'}$ -th sheet may have a same β as points on GBZ_{j_k} with $j_k \neq j_{k'}$, this point does not belong to the GBZ_{j_k} . In other words, there is no path on the Riemann surface to move a β from the neighbor of the origin to the infinity without crossing sub-GBZs. Therefore, all sub-GBZs together separate $\{\beta_1^{(j_1)}(E), \dots, \beta_M^{(j_M)}(E)\}$ and $\{\beta_{M+1}^{(j_{M+1})}(E), \dots, \beta_{2M}^{(j_{2M})}(E)\}$. When E crosses the OBC spectrum, there must be a point $\{\beta_M^{(j_M)}(E), E\}$ on the j_M -th sheet moving out of the GBZ_{j_M} while another point $\{\beta_{M+1}^{(j_{M+1})}(E), E\}$ on the j_{M+1} -th sheet moves into the $\text{GBZ}_{j_{M+1}}$. Then they exchange their root indexes M and $M + 1$. Eventually, all sub-GBZs on the Riemann surface still contains $\{\beta_1^{(j_1)}(E), \dots, \beta_M^{(j_M)}(E)\}$ inside. In conclusion, sub-GBZs on the Riemann surface are the boundary separating two groups of β roots of the characteristic equation Eq. (3).

We emphasize that the sub-GBZs are not a natural boundary if we view them just as close curves on the complex β -plane. Whereas the sub-GBZs may intersect with each other when viewed on the complex β -plane, they belong to different Riemann sheets and therefore are disconnected from the perspective of the Riemann surface. For example, in Fig. 2(a) and (c), it seems that the red sub-GBZ encloses β_3 when viewed in the complex β -plane. But the blue point β_3 belongs to the other sheet and stays outside of the blue sub-GBZ. This is fundamentally different from the situation in single-band models where there is only a single energy sheet, and consequently, a single GBZ loop. In multiband non-Hermitian systems, it is more natural to discuss the root distributions on the Riemann surface, instead of the complex β -plane.

From the perspective of the Riemann surface, we conclude that all sub-GBZs form a natural boundary separating $\{\beta_1^{(j_1)}(E), \dots, \beta_M^{(j_M)}(E)\}$ and $\{\beta_{M+1}^{(j_{M+1})}(E), \dots, \beta_{2M}^{(j_{2M})}(E)\}$ for arbitrary E not being on the OBC spectrum. We will use this fact to formulate multiband non-Hermitian Green's functions in the next section.

III. MULTIBAND GREEN'S FUNCTIONS

Considering a real-space OBC Hamiltonian H generated by Eq. (2), the Green's function is

$$\langle x, a | G(\omega) | y, b \rangle = \langle x, a | \frac{1}{\omega - H} | y, b \rangle, \quad (8)$$

where x, y are the spatial locations of different unit cells and a, b are the internal orbitals in each unit cell. For convenience,

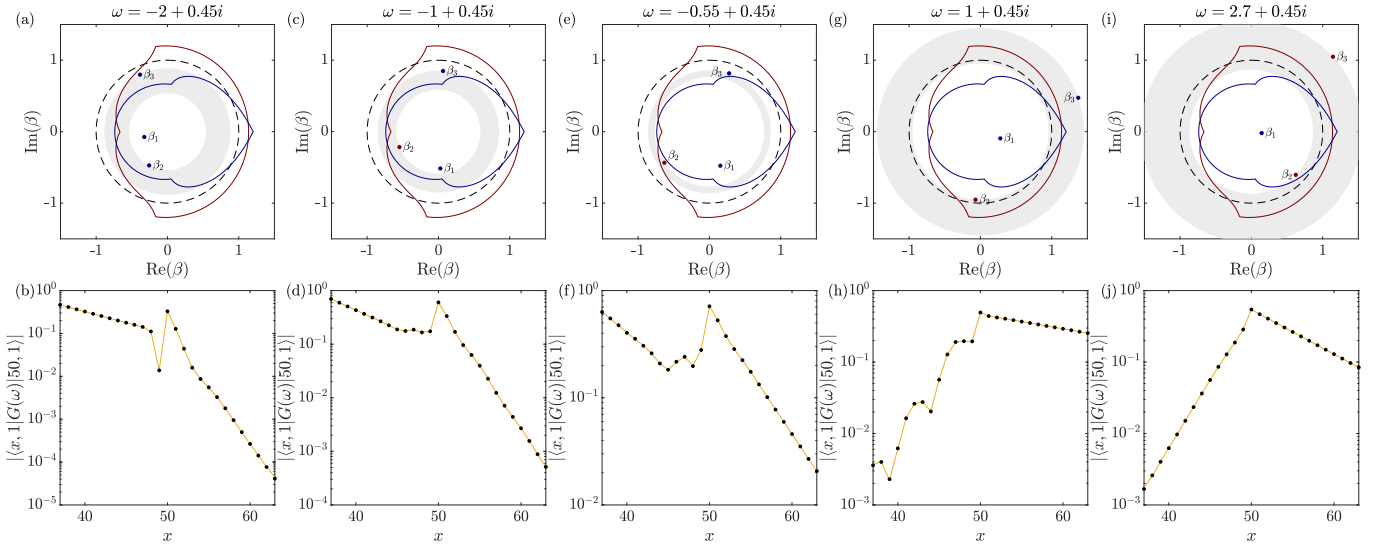


FIG. 2. The upper row shows sub-GBZs and the distribution of roots of $\det(\omega - h(\beta)) = 0$. Different colors of roots and sub-GBZs represent their sheet indexes. The fourth root is outside the plot. The gray circular region is $|\beta_M(\omega)| < R < |\beta_{M+1}(\omega)|$. The lower row displays the multiband Green's functions $\langle x, 1|G(\omega)|50, 1\rangle$ where the index 1 means the first orbital in the unit cell. Black dots come from numerical results on an open chain with $L = 100$; yellow lines are obtained from integrating Eq. (1). Each column is labeled by a different frequency shown above.

we take a complex frequency ω , the imaginary part of which is interpreted as the overall loss or gain added to the OBC Hamiltonian. Besides, ω is not taken from the OBC spectrum.

We shall make a connection between the OBC Green's function and an integral on the multiband GBZ. To do this, in Appendix A, we show that the OBC Green's function can be expressed as

$$\langle x, a|G(\omega)|y, b\rangle = \int_{|\beta|=R} \frac{d\beta}{2\pi i\beta} \beta^{x-y} \langle a| \frac{1}{\omega - h(\beta)} |b\rangle. \quad (9)$$

The integral contour is a circle with a radius R , which should satisfy $|\beta_M(\omega)| < R < |\beta_{M+1}(\omega)|$ with $\beta_M(\omega)$ and $\beta_{M+1}(\omega)$ being the middle two roots of $\det(\omega - h(\beta)) = 0$ (see Appendix A). This integral contour is not equivalent to the conventional Brillouin zone $|\beta| = 1$. The right-hand side is just the coefficients of the Laurent expansion of the complex function $\langle a| \frac{1}{\omega - h(\beta)} |b\rangle$ on the circular region $|\beta_M(\omega)| < R < |\beta_{M+1}(\omega)|$.

Note that the allowed values of R depend on ω , which is a shortcoming of the formula in Eq. (9). To use this formula, we need to specify the ω -dependent R first before calculating the integral. It is more natural to find a unique integral contour that is independent of ω . In single-band non-Hermitian systems and some simple multiband systems with overlapping sub-GBZs, it has been proved that OBC Green's functions are obtained from a contour integral on the GBZ [33]. Here we generalize the idea into multiband systems

One possible way for the generalization is that we may substitute the integral contour $|\beta| = R$ in Eq. (9) by a specific sub-GBZ. However, this is problematic (see Appendix B for a detailed discussion). This is because non-Hermitian Green's functions describe the response of the whole system to external perturbations, instead of just one of the energy bands.

Therefore, we expect to obtain a formula that takes all sub-GBZs into account.

A natural way to relate the circle $|\beta| = R$ to the sub-GBZs is to continuously deform the integral contour on the Riemann surface. To see this, we express Eq. (9) as

$$\langle x, a|G(\omega)|y, b\rangle = \int_{|\beta|=R} \frac{d\beta}{2\pi i\beta} \beta^{x-y} \sum_{j=1}^l \frac{\langle a|R_j, \beta\rangle \langle L_j, \beta|b\rangle}{\omega - E_j(\beta)} \quad (10)$$

In the above equation, $h(\beta)|R_j, \beta\rangle = E_j(\beta)|R_j, \beta\rangle$ and $\langle L_j, \beta| h(\beta) = \langle L_j, \beta| E_j(\beta)$. $E_j(\beta)$ is the eigenvalue of $h(\beta)$ on the j -th Riemann sheet. The left and right eigenvectors constitute the biorthogonal basis with $\langle L_j, \beta|R_j, \beta\rangle = \delta_{j,j'}$ and $\sum_{j=1}^l |R_j, \beta\rangle \langle L_j, \beta| = \mathbb{I}_{|\mathcal{X}|}$. For later convenience, we define $P_{j,ab}(\beta) = \langle a|R_j, \beta\rangle \langle L_j, \beta|b\rangle$ that is the matrix element of projection operators. Note that the integrand $\frac{P_{j,ab}(\beta)}{\omega - E_j(\beta)}$ is defined on the j -th sheet of the Riemann surface. Therefore, the poles on other sheets will not contribute to the integral on the j -th sheet.

We already know that sub-GBZs form a boundary separating $\{\beta_1(\omega), \dots, \beta_M(\omega)\}$ and $\{\beta_{M+1}(\omega), \dots, \beta_{2M}(\omega)\}$ on the Riemann surface. The same is true for the circle $|\beta| = R$ with $|\beta_M(\omega)| < R < |\beta_{M+1}(\omega)|$ if we view this circle as a collection of l identical copies on different sheets of the Riemann surface. Now we can freely deform the integral contour continuously from the $|\beta| = R$ loop to the corresponding sub-GBZ on the same sheet. Namely, $\int_{|\beta|=R} \frac{d\beta}{2\pi i\beta} \beta^{x-y} \frac{P_{j,ab}(\beta)}{\omega - E_j(\beta)} \rightarrow \int_{\text{GBZ}_j} \frac{d\beta}{2\pi i\beta} \beta^{x-y} \frac{P_{j,ab}(\beta)}{\omega - E_j(\beta)}$. The integral contour will not pass any poles when we track the deformation process on each Riemann sheet.

For example, as shown in Fig. 2, if we start from a circle in the gray region where $|\beta_M(\omega)| < R < |\beta_{M+1}(\omega)|$, deforming

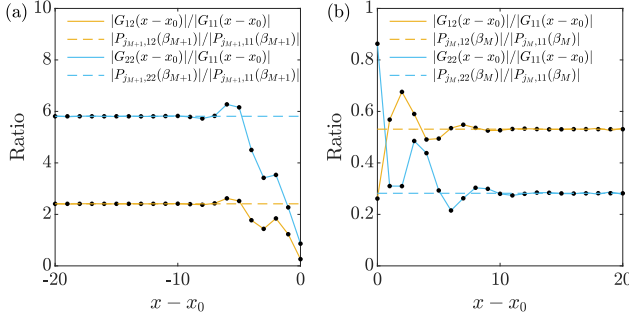


FIG. 3. The ratios between matrix elements of multiband Green's functions. We fix $\omega = -0.55 + 0.45i$. Black points are numerical results of an $L = 200$ chain and we take $x_0 = L/2$. We define $G_{ab}(x - x_0) = \langle x, a | \frac{1}{\omega - H} | x_0, b \rangle$ for the fixed frequency. The matrix elements of the j_k -th projection operator at $\beta_k^{(j_k)}(\omega)$ is $P_{j_k,ab}(\beta_k) = \langle a | R_{j_k}, \beta_k \rangle \langle L_{j_k}, \beta_k | b \rangle$ with $k = M + 1$ in (a) and $k = M$ in (b).

this loop to the red sub-GBZ will not pass any poles on the same sheet labeled by red points. While this deformation may cross blue poles on the other sheet [Fig. 2(a), (c) and (e)], it will not contribute to the integral on the sheet with red sub-GBZ. The same argument is true for the deformation into the blue sub-GBZ with examples in Fig. 2(e) and (g).

In the end, the OBC Green's functions of multiband non-Hermitian systems can be expressed as an integral on all sub-GBZs, as shown in Eq. (1) which is a central result of our work. Remarkably, this formula is free of artificially choosing ω -dependent integral contours as Eq. (9). This formula only depends on all sub-GBZs, unveiling that sub-GBZs play a fundamental role in the dynamics of multiband non-Hermitian systems.

The formula Eq. (1) goes back to the integral on the conventional Brillouin zone if the underlying system is Hermitian. It also naturally goes back to the single-band models [33]. If all the sub-GBZs of some simple multiband systems are overlapping on the β -plane, the formula in Eq. (1) goes back to Eq. (9) via replacing R by the coincident GBZ [33].

To facilitate applications of the formula Eq. (1), it is easy to show that the OBC Green's functions exhibit the asymptotic behaviors:

$$\langle x, a | G(\omega) | y, b \rangle \sim \begin{cases} P_{j_M,ab}(\beta_M(\omega))[\beta_M(\omega)]^{x-y}, & x \gg y; \\ P_{j_{M+1},ab}(\beta_{M+1}(\omega))[\beta_{M+1}(\omega)]^{-|x-y|}, & x \ll y. \end{cases} \quad (1')$$

This is the multiband generalization of the asymptotic behaviors of single-band Green's functions [33]. Notably, in addition to the asymptotically exponential behaviors, our formula also provides the ratios between different matrix elements of the multiband Green's function. Concretely, the ratios between $\langle x, a | G(\omega) | y, b \rangle$ with fixed x, y are given by the matrix elements of the projection operator $P_{j_k,ab}(\beta_k(\omega)) = \langle a | R_{j_k}, \beta_k(\omega) \rangle \langle L_{j_k}, \beta_k(\omega) | b \rangle$ at the pole $\beta_k(\omega)$ with $k = M + 1$ if $x \ll y$ and $k = M$ if $x \gg y$. As defined in the last section, j_k is the sheet index of $\{\beta_k(\omega), \omega\}$. The numerical results in Fig. 3 show the excellent agreement between ratios $\frac{\langle x, a | G(\omega) | y, b \rangle}{\langle x, a' | G(\omega) | y, b' \rangle}$ and $\frac{P_{j_{M+1},ab}(\beta_{M+1}(\omega))}{P_{j_M,a'b'}(\beta_{M+1}(\omega))}$ when $x \ll y$ (or $\frac{P_{j_M,ab}(\beta_M(\omega))}{P_{j_M,a'b'}(\beta_M(\omega))}$ when $x \gg y$).

when $x \gg y$). Therefore, our formula faithfully resolves the fine structures of multiband Green's functions between different orbitals. These fine structures cannot be seen from the formula Eq. (9).

IV. CONCLUSION

We study the multiband GBZ from the perspective of the Riemann surface and propose a proper formula of OBC Green's functions in multiband non-Hermitian systems. The exact formula Eq. (1) is an integral on the Riemann surface with the integral contours being the sub-GBZs on the Riemann sheets. These contours are independent of the frequency in the Green's functions. In fact, they are intrinsic geometrical construction of multiband non-Hermitian systems. The formula explicitly provides not only the asymptotic behaviors at the long distance but also the ratios between different orbitals. Our formula is applicable to studying non-Hermitian dynamics such as directional amplification in multiband systems.

ACKNOWLEDGMENT

We thank Fei Song and He-Ran Wang for helpful discussions and for comments on the manuscript. This work is supported by NSFC under Grant No. 12125405.

Appendix A: The proof of Eq. (9)

In this appendix, we show that the OBC multiband Green's functions can be expressed as

$$\langle x, a | G(\omega) | y, b \rangle = \int_{|\beta|=R} \frac{d\beta}{2\pi i \beta} \beta^{x-y} \langle a | \frac{1}{\omega - h(\beta)} | b \rangle. \quad (A1)$$

The integral contour is a circle with a radius R , where $|\beta_M(\omega)| < R < |\beta_{M+1}(\omega)|$ with $\beta_M(\omega)$ and $\beta_{M+1}(\omega)$ being the M -th and $(M + 1)$ -th roots of $\det(\omega - h(\beta)) = 0$.

Why is this circular region so special? To answer this question, we use the language of Toeplitz matrices and generalize the argument in Ref. [33] into multiband systems. Given a matrix-valued Laurent polynomial $f(\beta) = \sum_n c_n \beta^n$ with c_n being $l \times l$ coefficient matrices, a block Toeplitz matrix $T(f)$ is defined as $T_{jk}(f) = c_{k-j} = \int_{|\beta|=R} \frac{d\beta}{2\pi i \beta} \beta^{j-k} f(\beta)$ for an arbitrary R . We denote an $l \times l$ block of the whole Toeplitz matrix as $T_{jk}(f)$. In other words, $T(f)$ is expressed as the following block structure:

$$T(f) = \begin{pmatrix} c_0 & c_1 & c_2 & \cdots \\ c_{-1} & c_0 & c_1 & \ddots \\ c_{-2} & c_{-1} & c_0 & \ddots \\ \vdots & \ddots & \ddots & \ddots \end{pmatrix}. \quad (A2)$$

This is just a real-space Hamiltonian if we interpret $f(\beta)$ as a non-Bloch Hamiltonian $h(\beta)$ in Eq. (2). The OBC Hamiltonian H is obtained by truncating $T(h)$ as an $Ll \times Ll$ matrix with L being the number of unit cells.

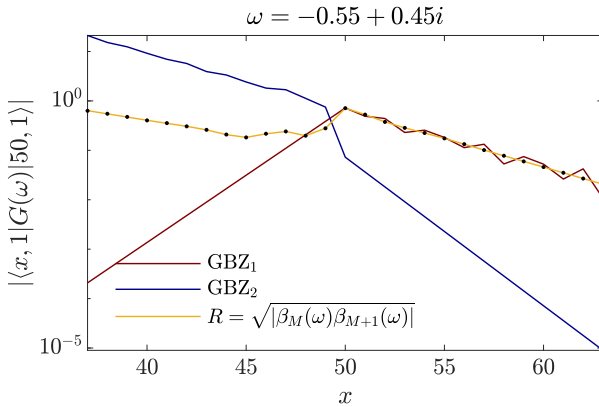


FIG. 4. The failure of the formulas based on a specific sub-GBZ. The index 1 in $\langle x, 1|G(\omega)|50, 1\rangle$ labels the first orbital in the unit cell. The yellow line is calculated by Eq. (A1) with a circle contour $R = \sqrt{|\beta_M(\omega)\beta_{M+1}(\omega)|}$, which is in excellent agreement with numerical results from an $L = 100$ chain. The red (blue) line comes from Eq. (B1) by choosing GBZ₁ (GBZ₂) to be the integral contour. The artificial choice of sub-GBZs fails to predict non-Hermitian Green's functions.

Now let us take two block Toeplitz matrices $T(f_1)$ and $T(f_2)$ generated by two $l \times l$ matrix-valued Laurent polynomials $f_1(\beta) = \sum_n a_n \beta^n$ and $f_2(\beta) = \sum_n b_n \beta^n$ respectively. There is a simple identity $T(f_1)T(f_2) = T(f_1f_2)$ coming from $\sum_k T_{ik}(f_1)T_{kj}(f_2) = \sum_k a_{k-i}b_{j-k} = (f_1f_2)_{j-i} = T_{ij}(f_1f_2)$. Strictly speaking, the identity is an approximation without taking the boundary contributions into account. Such boundary correction is exponentially small in the bulk compared to $(f_1f_2)_{j-i}$. Hence, we ignore the boundary effect here. An immediate consequence of the identity is that $T(f)T(f^{-1}) = 1$, namely, $[T(f)]^{-1} = T(f^{-1})$. To get the OBC Green's functions, we replace $f(\beta)$ by $\omega - h(\beta)$ to get the expression $[T(\omega - h(\beta))]^{-1} = T(\frac{1}{\omega - h(\beta)})$. The matrix elements $\langle x, a|T(\omega - h(\beta))|^{-1}|y, b\rangle$ are given by the Laurent expansion of $\langle a|\frac{1}{\omega - h(\beta)}|b\rangle$, as shown in Eq. (A1). Because $\frac{1}{\omega - h(\beta)}$ has poles at the roots of $\det(\omega - h(\beta)) = 0$, we shall specify which R is proper for the Laurent expansion.

Consider a smooth interpolation $f_s(\beta)$ where $f_{s=1}(\beta) = f(\beta)$ and $f_{s=0}(\beta) = \mathbb{I}_{l \times l}$. The Toeplitz matrix generated by $f_{s=0}(\beta) = \mathbb{I}_{l \times l}$ trivially satisfies $T(f_{s=0})T(f_{s=0}^{-1}) = 1$. Then the smooth interpolation of $[f_s(\beta)]^{-1}$ from $s = 0$ to $s = 1$ provides the proper expansion of $[f_{s=1}(\beta)]^{-1}$. This requires that $f_s(\beta) \neq 0$ on the integral circle $|\beta| = R$. The topological winding number $W_s = \frac{1}{2\pi} \int_{|\beta|=R} d\log[\det(f_s(\beta))] = 0$ remains unchanged during

the smooth interpolation because it has a vanishing value at $s = 0$. Now we take $f(\beta) = \omega - h(\beta)$ to discuss multiband non-Hermitian Green's functions. Considering that $\det(\omega - h(\beta)) = \frac{C_M}{\beta^M} \prod_{k=1}^{2M} (\beta - \beta_k(\omega))$ with $\beta_{k=1, \dots, 2M}(\omega)$ being $2M$ roots ordered by their norms, the requirement of zero winding number leads to the radius R satisfying $|\beta_M(\omega)| < R < |\beta_{M+1}(\omega)|$. In the end, we get back to the integral form in Eq. (9) of the main text. A more formal proof can be found in Ref. [25].

Appendix B: The Failure of the formulas based on a specific sub-GBZ

In the main text, we mentioned that substituting the integral contour $|\beta| = R$ in Eq. (9) by a specific sub-GBZ is problematic. According to this approach, the Green's function formula would be an integral on GBZ_j for a certain j [45]:

$$\langle x, a|G(\omega)|y, b\rangle \stackrel{?}{=} \int_{\text{GBZ}_j} \frac{d\beta}{2\pi i \beta} \beta^{x-y} \langle a| \frac{1}{\omega - h(\beta)} |b\rangle. \quad (\text{B1})$$

In this appendix, we demonstrate the failure of this plausible formula in more detail. The results in Fig. 4 show that integrating along a specific sub-GBZ does not predict the numerical values of multiband non-Hermitian Green's functions. This mismatch can be explained by contour deformation on the complex β -plane.

As shown in Fig. 2 of the main text, $|\beta| = R$ lies in the gray circular region between $|\beta_2(\omega)|$ and $|\beta_3(\omega)|$. Deforming $|\beta| = R$ on the complex β -plane into the red sub-GBZ in Fig. 2(a) and (c) or into the blue sub-GBZ in Fig. 2(g) will inevitably cross the poles of $\frac{1}{\omega - h(\beta)}$ at $\beta_3(\omega)$ or $\beta_2(\omega)$ respectively. This process changes the integral results of Eq. (B1). The situation is even worse in Fig. 2(e) (the same parameter as Fig. 4) where the deformation to either red or blue sub-GBZ will always cross poles. Then Eq. (B1) with artificially choosing one of the sub-GBZs will yield problematic results.

A more physical reason of the failure of the above extension is that non-Hermitian Green's functions describe the response of the whole system to external perturbations, instead of just one of the energy bands. Therefore, the formula based on a specific sub-GBZ fails in predicting the Green's functions in general multiband non-Hermitian systems.

The formula Eq. (B1) is only applicable to special cases such as Fig. 2(i). In these cases, there is no pole between different sub-GBZs viewed on the complex β -plane. Hence, all sub-GBZs are equivalent to each other when we calculate the integral along them.

[1] Y. Ashida, Z. Gong, and M. Ueda, Non-hermitian physics, *Advances in Physics* **69**, 249 (2020).

[2] E. J. Bergholtz, J. C. Budich, and F. K. Kunst, Exceptional topology of non-hermitian systems, *Rev. Mod. Phys.* **93**, 015005 (2021).

[3] S. Yao and Z. Wang, Edge states and topological invariants of non-hermitian systems, *Phys. Rev. Lett.* **121**, 086803 (2018).

[4] S. Yao, F. Song, and Z. Wang, Non-hermitian chern bands, *Phys. Rev. Lett.* **121**, 136802 (2018).

[5] F. K. Kunst, E. Edvardsson, J. C. Budich, and E. J. Bergholtz, Biorthogonal bulk-boundary correspondence in non-hermitian systems, *Phys. Rev. Lett.* **121**, 026808 (2018).

[6] V. M. Martinez Alvarez, J. E. Barrios Vargas, and L. E. F. Foa Torres, Non-hermitian robust edge states in one dimension:

Anomalous localization and eigenspace condensation at exceptional points, *Phys. Rev. B* **97**, 121401 (2018).

[7] C. H. Lee and R. Thomale, Anatomy of skin modes and topology in non-hermitian systems, *Phys. Rev. B* **99**, 201103 (2019).

[8] L. Xiao, T. Deng, K. Wang, G. Zhu, Z. Wang, W. Yi, and P. Xue, Non-hermitian bulk-boundary correspondence in quantum dynamics, *Nature Physics* **16**, 761 (2020).

[9] T. Helbig, T. Hofmann, S. Imhof, M. Abdelghany, T. Kiessling, L. Molenkamp, C. Lee, A. Szameit, M. Greiter, and R. Thomale, Generalized bulk-boundary correspondence in non-hermitian topoelectrical circuits, *Nature Physics* **16**, 747 (2020).

[10] A. Ghatak, M. Brandenbourger, J. van Wezel, and C. Coulais, Observation of non-hermitian topology and its bulk-edge correspondence in an active mechanical metamaterial, *Proceedings of the National Academy of Sciences* **117**, 29561 (2020).

[11] S. Weidemann, M. Kremer, T. Helbig, T. Hofmann, A. Stegmaier, M. Greiter, R. Thomale, and A. Szameit, Topological funneling of light, *Science* **368**, 311 (2020).

[12] W. Wang, X. Wang, and G. Ma, Non-hermitian morphing of topological modes, *Nature* **608**, 50 (2022).

[13] X. Zhang, T. Zhang, M.-H. Lu, and Y.-F. Chen, A review on non-hermitian skin effect, *Advances in Physics: X* **7**, 2109431 (2022), <https://doi.org/10.1080/23746149.2022.2109431>.

[14] K. Ding, C. Fang, and G. Ma, Non-hermitian topology and exceptional-point geometries, *Nature Reviews Physics* **1**, 1 (2022).

[15] R. Lin, T. Tai, L. Li, and C. H. Lee, Topological non-hermitian skin effect, *arXiv preprint arXiv:2302.03057* (2023).

[16] K. Yokomizo and S. Murakami, Non-bloch band theory of non-hermitian systems, *Phys. Rev. Lett.* **123**, 066404 (2019).

[17] F. Song, S. Yao, and Z. Wang, Non-hermitian topological invariants in real space, *Phys. Rev. Lett.* **123**, 246801 (2019).

[18] Z. Yang, K. Zhang, C. Fang, and J. Hu, Non-hermitian bulk-boundary correspondence and auxiliary generalized brillouin zone theory, *Phys. Rev. Lett.* **125**, 226402 (2020).

[19] T.-S. Deng and W. Yi, Non-bloch topological invariants in a non-hermitian domain wall system, *Phys. Rev. B* **100**, 035102 (2019).

[20] S. Longhi, Non-bloch-band collapse and chiral zener tunneling, *Phys. Rev. Lett.* **124**, 066602 (2020).

[21] K. Kawabata, N. Okuma, and M. Sato, Non-bloch band theory of non-hermitian hamiltonians in the symplectic class, *Phys. Rev. B* **101**, 195147 (2020).

[22] T. Liu, Y.-R. Zhang, Q. Ai, Z. Gong, K. Kawabata, M. Ueda, and F. Nori, Second-order topological phases in non-hermitian systems, *Phys. Rev. Lett.* **122**, 076801 (2019).

[23] C. H. Lee, L. Li, R. Thomale, and J. Gong, Unraveling non-hermitian pumping: Emergent spectral singularities and anomalous responses, *Phys. Rev. B* **102**, 085151 (2020).

[24] Y. Yi and Z. Yang, Non-hermitian skin modes induced by on-site dissipations and chiral tunneling effect, *Phys. Rev. Lett.* **125**, 186802 (2020).

[25] H.-Y. Wang, F. Song, and Z. Wang, Amoeba formulation of the non-hermitian skin effect in higher dimensions, *arXiv preprint arXiv:2212.11743* (2022).

[26] F. Song, S. Yao, and Z. Wang, Non-hermitian skin effect and chiral damping in open quantum systems, *Phys. Rev. Lett.* **123**, 170401 (2019).

[27] S. Longhi, Probing non-hermitian skin effect and non-bloch phase transitions, *Phys. Rev. Research* **1**, 023013 (2019).

[28] S. Longhi, Non-Bloch PT symmetry breaking in non-Hermitian photonic quantum walks, *Optics Letters* **44**, 5804 (2019).

[29] L. Xiao, T. Deng, K. Wang, Z. Wang, W. Yi, and P. Xue, Observation of non-bloch parity-time symmetry and exceptional points, *Phys. Rev. Lett.* **126**, 230402 (2021).

[30] W.-T. Xue, Y.-M. Hu, F. Song, and Z. Wang, Non-hermitian edge burst, *Phys. Rev. Lett.* **128**, 120401 (2022).

[31] S. Longhi, Self-healing of non-hermitian topological skin modes, *Phys. Rev. Lett.* **128**, 157601 (2022).

[32] S. Longhi, Non-hermitian skin effect and self-acceleration, *Phys. Rev. B* **105**, 245143 (2022).

[33] W.-T. Xue, M.-R. Li, Y.-M. Hu, F. Song, and Z. Wang, Simple formulas of directional amplification from non-bloch band theory, *Phys. Rev. B* **103**, L241408 (2021).

[34] C. C. Wanjura, M. Brunelli, and A. Nunnenkamp, Topological framework for directional amplification in driven-dissipative cavity arrays, *Nature communications* **11**, 3149 (2020).

[35] N. Okuma and M. Sato, Non-hermitian skin effects in hermitian correlated or disordered systems: Quantities sensitive or insensitive to boundary effects and pseudo-quantum-number, *Phys. Rev. Lett.* **126**, 176601 (2021).

[36] L. Li, S. Mu, C. H. Lee, and J. Gong, Quantized classical response from spectral winding topology, *Nature communications* **12**, 5294 (2021).

[37] L. Li, C. H. Lee, S. Mu, and J. Gong, Critical non-Hermitian skin effect, *Nature Communications* **11**, 5491 (2020).

[38] Z. Yang, K. Zhang, C. Fang, and J. Hu, Non-hermitian bulk-boundary correspondence and auxiliary generalized brillouin zone theory, *Phys. Rev. Lett.* **125**, 226402 (2020).

[39] Y. Fu and Y. Zhang, Anatomy of open-boundary bulk in multi-band non-hermitian systems, *Phys. Rev. B* **107**, 115412 (2023).

[40] C. Liu, L. Li, and J. An, Topological invariant for multi-band non-hermitian systems with chiral symmetry, *arXiv preprint arXiv:2303.05053* (2023).

[41] C.-H. Liu, K. Zhang, Z. Yang, and S. Chen, Helical damping and dynamical critical skin effect in open quantum systems, *Phys. Rev. Research* **2**, 043167 (2020).

[42] K. Yokomizo and S. Murakami, Scaling rule for the critical non-hermitian skin effect, *Phys. Rev. B* **104**, 165117 (2021).

[43] K. Zhang, Z. Yang, and C. Fang, Correspondence between winding numbers and skin modes in non-hermitian systems, *Phys. Rev. Lett.* **125**, 126402 (2020).

[44] N. Okuma, K. Kawabata, K. Shiozaki, and M. Sato, Topological origin of non-hermitian skin effects, *Phys. Rev. Lett.* **124**, 086801 (2020).

[45] Recently, the formula based on a specific sub-GBZ is adopted in Ref. [39].